Filtration Modeling of a Plate-And-Frame-Press

by

Scott A. Wells[1]

Abstract

The porosity distribution and filtrate production during cake filtration in a plate-and-frame filter press were simulated mathematically. The model considered filtration that occurs after the filling process, not filtration that occurs as the suspension fills the cell. Governing equations for the temporal porosity distribution were developed for a plate-and-frame press. The governing equations were solved numerically using an alternating-direction-implicit scheme. Appropriate initial and boundary conditions were determined based on characteristics of the plate-and-frame press and of the suspension properties. Predicted porosity and velocity distributions were calculated for assumed constitutive parameters.

Key words:

[1] Professor of Civil Engineering, Department of Civil Engineering, Portland State University, Portland, Oregon 97207-0751 USA, (503) 725-4276 FAX (503) 725-5950, e-mail: scott@eas.pdx.edu; web page: www.ce.pdx.edu/~wellss

plate-and-frame press, surface filtration, mathematical modeling of dewatering, expression, constitutive relationships, dewatering, sludge dewatering

INTRODUCTION

Plate-and-frame presses are used frequently in solid-liquid separation processes (Avery, 1988). After emptying the cake from a cell of a plate-and-frame press from a prior filtration cycle, a suspension is pumped under pressure into an empty cell. During this period, some filtration occurs. After filling the cell, filtration proceeds as the pump pressure increases. The model described in this study evaluated filtration that occurs after the filling process. Figure 1 shows an individual plate-and-frame press cell used for the modeling study.

THEORETICAL BACKGROUND

Governing equations for cake filtration include solid and liquid continuity and the reduced forms of the solid and liquid momentum equations (Willis, 1983) assuming that the inertial and gravity terms of the liquid and solid phase and the solid-solid shear stresses are negligible and that $\partial / \partial x=0$ (where x is the spatial coordinate into the plane of Figure 1):

$$\frac{\partial e}{\partial t} = \frac{\partial}{\partial y}\left(e V_{ly}\right) + \frac{\partial}{\partial z}\left(e V_{lz}\right) \qquad \mathbf{1}$$

$$\frac{\partial[1-\varepsilon]}{\partial t} = \frac{\partial}{\partial y}\left([1-\varepsilon]V_{sy}\right) + \frac{\partial}{\partial z}\left([1-\varepsilon]V_{sz}\right) \qquad \mathbf{2}$$

$$k_y \frac{dp}{dy} = \varepsilon\mu(V_{ly} - V_{sy}) \qquad \mathbf{3}$$

$$k_z \frac{dp}{dz} = \varepsilon\mu(V_{lz} - V_{sz}) \qquad \mathbf{4}$$

$$\sigma' + p = \Delta p \qquad \mathbf{5}$$

where ε is the porosity [-], V_l is the liquid velocity [cm/s], V_s is the solid velocity [cm/s], σ' is the effective stress [kPa], p is the porewater pressure [kPa], t is time [s], y and z are spatial coordinates [cm], Δp is the total applied pressure [kPa].

By taking the derivative of Equation 3 with respect to y and the derivative of Equation 4 with respect to x, adding the resulting equations and substituting Equation 1,

$$\mu\left[\frac{\partial\varepsilon}{\partial t} - \frac{\partial(\varepsilon V_{sy})}{\partial y} - \frac{\partial(\varepsilon V_{sz})}{\partial z}\right] = \frac{\partial}{\partial y}\left(k_y \frac{\partial p}{\partial y}\right) + \frac{\partial}{\partial z}\left(k_z \frac{\partial p}{\partial z}\right) \qquad \mathbf{6}$$

Using the definition of the constitutive property that $m_v = -\frac{\partial\varepsilon}{\partial\sigma'} = \frac{\partial\varepsilon}{\partial p}$ and the definition of a partial differential such that $\frac{\partial p}{\partial y} = \frac{\partial p}{\partial\varepsilon}\frac{\partial\varepsilon}{\partial y}$ and $\frac{\partial p}{\partial z} = \frac{\partial p}{\partial\varepsilon}\frac{\partial\varepsilon}{\partial z}$, and assuming that $\partial\varepsilon/\partial t \gg \partial(\varepsilon V_{sy})/\partial y$ and $\partial(\varepsilon V_{sz})/\partial z$ (Voroboyov, 1993), Equation 6 becomes

$$\frac{\partial\varepsilon}{\partial t} = \frac{\partial}{\partial y}\left[\frac{k_y}{m_{v_y}\mu}\frac{\partial\varepsilon}{\partial y}\right] + \frac{\partial}{\partial z}\left[\frac{k_z}{m_{v_z}\mu}\frac{\partial\varepsilon}{\partial z}\right] \qquad \mathbf{7}$$

The boundary conditions for the domain shown in Figure 1 are

$$\varepsilon(y,z,t=0)=\varepsilon(y,z)_{initial} \qquad \mathbf{8}$$

$$\left.\frac{\partial \varepsilon}{\partial y}\right|_{y=L,z,t}=0 \qquad \mathbf{9}$$

$$\varepsilon(y,z=0 \textit{ and } z=H,t)=\varepsilon_{o}(t) \qquad \mathbf{10}$$

$$\varepsilon(y=0,z,t)=\varepsilon_{i} \qquad \mathbf{11}$$

where ε_i is the initial porosity of the suspension (constant over time if the porosity of the feed solution remains constant and no filtration occurs in the manifold to the individual filtration cells), ε_o is the terminal porosity along the filter medium (a function of time because the applied pressure changes as the pressure output of the pump supplying the filter cells varies), and $\varepsilon_{initial}$ is the initial porosity distribution in the filtration cell after the filling process.

NUMERICAL SOLUTION

The governing equation was solved by finite difference methods. The spatial domain was divided into equally spaced grid points in the y and z directions. Since the terms, $\frac{k_z}{\mu m_{v_z}}$ and $\frac{k_y}{\mu m_{v_y}}$, were non-linear, direct solution techniques resulting in excessive computational time were not used. Defining these terms as

$$\beta_y = \frac{k_y}{\mu m_{v_y}} \qquad \textbf{12}$$

and

$$\beta_z = \frac{k_z}{\mu m_{v_z}}, \qquad \textbf{13}$$

linearization of the term β at the n+1 time step was accomplished by using a Taylor series expansion neglecting higher order terms such that

$$\beta^{n+1} \approx \beta^{n} + \Delta t \left.\frac{\partial \beta}{\partial t}\right|^{n} \qquad \textbf{14}$$

where n is the time level of the numerical solution and Δt is the time step.

In this case, using an approximation for $\partial\beta/\partial t$ at the n time level by using a backward difference in time [such as, $(\beta^{n}-\beta^{n-1})/\Delta t$] eliminated the non-linearity, such that

$$\beta^{n+1} \approx 2\beta^{n} - \beta^{n-1}. \qquad \textbf{15}$$

The alternating-direction-implicit technique (ADI) was used for solving the linearized partial differential equation (Anderson et al, 1984). This technique splits the solution into 2 parts (sweeping along rows of y and columns of x) thus accelerating convergence of the solution.

The first difference equation for advancing n+1/2 time steps was

$$\varepsilon_{i,j}^{n+1/2}[1+0.5\alpha_y(\beta^n_{y_{i+1/2,j}}+\beta^n_{y_{i-1/2,j}})]+$$

$$\varepsilon_{i+1,j}^{n+1/2}[-0.5\alpha_y\beta^n_{y_{i+1/2,j}}]+\varepsilon_{i-1,j}^{n+1/2}[-0.5\alpha_y\beta^n_{y_{i-1/2,j}}]=$$

$$\varepsilon_{i,j}^{n}[1-0.5\alpha_z\beta^n_{z_{i,j-1/2}}-0.5\alpha_z\beta^n_{z_{i,j+1/2}}]+$$

$$\varepsilon_{i,j-1}^{n}[0.5\alpha_z\beta^n_{z_{i,j-1/2}}]+\varepsilon_{i,j+1}^{n}[0.5\alpha_z\beta^n_{z_{i,j+1/2}}] \qquad \mathbf{16}$$

After the sweep of each row, the second equation for advancing the iteration to the n+1 time step was

$$e_{i,j}^{n+1}[1+0.5a_z(b^{n+1/2}_{z_{i,j+1/2}}+b^{n+1/2}_{z_{i,j-1/2}})]+$$

$$e_{i,j+1}^{n+1}[-0.5a_z b^{n+1/2}_{z_{i,j+1/2}}]+e_{i,j-1}^{n+1}[-0.5a_z b^{n+1/2}_{z_{i,j-1/2}}]=$$

$$e_{i,j}^{n+1/2}[1-0.5a_y b^{n+1/2}_{y_{i-1/2,j}}-0.5a_y b^{n+1/2}_{y_{i+1/2,j}}]+$$

$$e_{i-1,j}^{n+1/2}[0.5a_y b^{n+1/2}_{y_{i-1/2,j}}]+e_{i+1,j}^{n+1/2}[0.5a_y b^{n+1/2}_{y_{i+1/2,j}}] \qquad \mathbf{17}$$

where $a_y=\frac{\Delta t}{\Delta y^2}$ and $a_z=\frac{\Delta t}{\Delta z^2}$.

After advancing to the n+1 time level, iteration was continued until the solution converged. The convergence criteria was set by the user. The iteration proceeded by setting the ε^{n+1} value to ε^{p+1}, where p was the iteration level.

DETERMINATION OF THE TERMINAL POROSITY AS A FUNCTION OF TIME

The value of ε_o, the boundary condition along the z=0 and z=H axes, was a function of time because of fluid pressure changes from the pump supplying the filter cells. As suggested by Vorobjov (1993), a typical characteristic curve for a pump was necessary as input to the model. The pump characteristic curve could be determined as a polynomial function of suspension flow rate, Q (cm^3/s):

$$p(kPa) = p_a(kPa) + p_b\, Q + p_c\, Q^2 \qquad \textbf{18}$$

where p is the porewater pressure supplied by the pump in kPa, p_a (kPa), p_b ($kPa/cm^3/s$), and p_c ($kPa/cm^6/s^2$) are empirical parameters. Figure 2 shows a typical characteristic curve for a pump.

The maximum applied pressure could be determined by taking the derivative of the Equation 18, dp/dQ = 0, and solving for Q_{max} at p_{max}. Then $Q_{max} = \frac{-p_b}{2p_c}$ and p_{max} was determined by substituting this result into Equation 18.

In the model the flow of the suspension to the plates after the filling process would be equal to the total filtrate production from all the filter cells.

DETERMINATION OF THE LIQUID VELOCITY AND FILTRATE PRODUCTION

The technique to calculate these quantities was similar to that used by Wells (1991) where the momentum Equations 3 and 4 were inverted to solve for V_{lz} and V_{ly} such as

$$V_{ly} = \frac{k_y}{\boldsymbol{em}} \frac{dp}{dy} = \frac{k_y}{\boldsymbol{em} m_{v_y}} \frac{\partial \boldsymbol{e}}{\partial y} \quad \textbf{19}$$

$$V_{lz} = \frac{k_z}{\boldsymbol{em}} \frac{dp}{dz} = \frac{k_z}{\boldsymbol{em} m_{v_z}} \frac{\partial \boldsymbol{e}}{\partial z} \quad \textbf{20}$$

These equations were put into finite difference form and solved from the porosity distribution. The total filtrate production, Q in cm^3/s, was calculated from

$$Q = 2\, N\, W \sum_{i=1}^{i=ny} V_{z=0_i}\, \Delta y\, \boldsymbol{e}_o \quad \textbf{21}$$

where W is the cell width in cm, N is the number of filter cells for the entire filter press, the "2" is to account for the filtrate production along the z=H boundary, i is the number of model cells along the y-axis, and ny is the number of grid cells along y.

CONSTITUTIVE RELATIONSHIPS

The model used functional forms of constitutive relationships from Wells (1991) and Vorobjov et al. (1993) . These relationships described the stress-strain relationships of the cake. Relationships between the cake porosity (or void ratio) and effective stress and between the cake porosity and permeability (or similarly between cake resistance and porewater pressure) were necessary as input to the mathematical model.

Those relationships used by Wells (1991) were exponential functions where

$$m_{v\,y,z} = -\frac{\partial e}{\partial \sigma'} = \frac{\partial e}{\partial p} = ava_{y,z}\exp(avb_{y,z}e) \qquad \mathbf{22}$$

and

$$k_{y,z} = pka_{y,z}\exp(pkb_{y,z}e) \qquad \mathbf{23}$$

where ava [gm/cm/s²], avb [-], pka [cm²], and pkb [-] are empirical coefficients. The subscripts in y and z indicate that different relationships could be used in y than in z.

The terminal porosity ε_o was determined by integrating the stress-strain relationship for the solid phase from Equation 22, such as

$$\int_{\Delta p}^{p} \partial p = \int_{e_i}^{e} \frac{\partial e}{m_v} \qquad \mathbf{24}$$

After integration and simplification, the porosity at any porewater pressure p was then

$$e = -\frac{1}{avb}\ln\left[(ava\ avb\ (\Delta p - p) + \exp(-avb\ e_i)\right] \qquad \mathbf{25}$$

The terminal porosity was determined by setting p=0 kPa in the above equation.

A power-law relationship used by Vorobjov et al. (1993) was of the form

$$r_{y,z} = r_{o_{y,z}}\left(\frac{\sigma'}{\Delta p}\right)^{S} = k_{y,z}^{-1} \qquad \mathbf{26}$$

and

$$G = -(1+e)\frac{\partial \sigma'}{\partial e} = G_o(\frac{\sigma'}{\Delta p})^n \quad \text{or} \quad m_v = \frac{e^2}{1+e}G^{-1} = \frac{\varepsilon^2}{1-\varepsilon}\frac{(\frac{\Delta p}{\sigma'})^n}{G_o} \qquad \mathbf{27}$$

where G is the cake compressibility modulus, kPa; e is the void ratio, $\varepsilon/(1-\varepsilon)$, r is the resistance [$m^{-2}$], r_o is an empirical coefficient [m^{-2}], G_o is an empirical coefficient [kPa], and S is the compressibility coefficient [-].

The relationship between void ratio and effective stress can be obtained by integrating Equation 27 from the initial void ratio to an arbitrary void ration e with n=1, such that

$$-\int_{e_o}^{e}\frac{\partial e}{1+e} = \int_{\Delta p}^{\sigma'}\frac{\partial \sigma'}{G} = \frac{\Delta p}{G_o}\int_{\Delta p}^{\sigma'}\frac{\partial \sigma'}{\sigma'} \qquad \mathbf{28}$$

Then, after simplification, the ratio of Δp over effective stress can be determined as a function of the void ratio or porosity as

$$\frac{\Delta p}{\sigma'} = \left[\frac{1+e}{1+e_o}\right]^{\frac{G_o}{\Delta p}} = \left[\frac{1-\varepsilon_o}{1-\varepsilon}\right]^{\frac{G_o}{\Delta p}} \qquad \mathbf{29}$$

This constitutive relationship has the undesirable quality that the porosity or void ratio at p=0 or $\sigma'=\Delta p$ cannot be determined. This occurs because the integration of Equation 28 cannot be made between the limits of e_i to e (or ε_i to ε) as was performed in the integration of Equation 24. For example, at $e=e_i$, $\sigma'=0$, and the integral of Equation 28 is undefined. One way to approximate this was to take the limits of integration in

Equation 28 from e to e_i and from σ' to σ_{small}, where σ_{small} is an arbitrary, very small, non-zero stress. Carrying out the integration, substituting σ'=Δp, and simplifying resulted in

$$e_o = (1 - e_i)\left(\frac{\boldsymbol{s}_{small}}{\Delta p}\right)^{\frac{-\Delta p}{G_o}} - 1 \qquad \textbf{30}$$

or in terms of porosity,

$$\varepsilon_o = 1 - (1 - \varepsilon_i)\left(\frac{\sigma_{small}}{\Delta p}\right)^{\frac{-\Delta p}{G_o}} \qquad \textbf{31}$$

(Note that because of this problem in determining ε_o with the second set of constitutive parameters, a model based on effective stress, σ', rather than porosity, ε, would be more appropriate since no simplifying assumptions regarding σ_{small} would have to be made unless one wanted to convert the σ' values to ε values.)

In order to illustrate the functional dependence on porosity, Figures 3 and 4 show comparisons of the exponential and the power law constitutive relationships for some hypothetical parameters. Figure 5 shows how the effective stress - porosity relationship varies as the value of σ_{small} is varied using the power function constitutive relationship. The terminal porosity (and hence the ε-σ' relationship) is a strong function of σ_{small}.

POROSITY INITIAL CONDITION

The initial porewater pressure (or porosity) distribution in the filter plate cell at the end of the filling cycle is required for the numerical solution. Since this initial distribution was unknown, it was estimated using different functional forms of the initial porosity distribution that would satisfy the boundary conditions at the beginning of filtration. One of these initial pressure distributions evaluated was a parabolic distribution in z from z=0 to z=H/2 (the centerline). This pressure distribution was assumed to be of the form

$$p(kPa) = a + bz + cz^2 \qquad \mathbf{32}$$

where a [kPa], b [kPa/cm], and c [kPa/cm^2] are empirical coefficients and z is the distance from z=0 in cm. Note that dp/dz = b + 2cz. To satisfy the boundary conditions that $p=p_{applied}$ (a fraction of the theoretical maximum pressure or the porewater pressure delivered by the pump at the end of the filling period) at z=H/2 and p=0 at z=0, the coefficient "a" must be zero and (using H/2=h)

$$c = \frac{p_{applied} - bh}{h^2} \qquad \mathbf{33}$$

Because the filtrate production must always be non-zero and positive, the condition that dp/dz > 0 required that b>0 and $b < \frac{2\,p_{applied}}{h}$. The filtrate production along z=0 was then at the beginning of the model simulation

$$V(y, z = 0, t = 0) = \frac{k}{me}\frac{dp}{dz}\bigg|_{z=0} = \frac{k}{me}b\bigg|_{z=0} \qquad \mathbf{34}$$

Figure 6 shows the variation in pressure with distance from the filter medium for a $p_{applied}$ of 175 kPa satisfying both the boundary conditions at each end of the domain and the above conditions. The corresponding initial porosity distribution is shown in Figure 7. Using Equation 34, the variation of filtrate production with the parameter "b" is shown in Figure 8.

DETERMINATION OF MODEL PARAMETERS

Data required for the model included the following: (1) relationship between permeability and porosity (such as parameters pka and pkb in Equation 23), (2) relationship between porewater pressure (or effective stress) and porosity (such as ava and avb as in Equation 22), (3) relationship between pump pressure and suspension flow rate (pump characteristic curve, where p_a, p_b, and p_c are curve parameters as in Equation 18), and (4) the pressure differential at the initiation of expression ($p_{initial}$, some fraction of the total pressure differential $p_{applied}$).

Once $p_{initial}$ (at t=0) is estimated, the initial filtrate flow rate at t=0 can be calculated from inverting Equation 18, such that

$$Q = \frac{-\frac{p_b}{p_c} \pm \sqrt{(\frac{p_b}{p_c})^2 - 4(\frac{p_a - p_{initial}}{p_c})}}{2} \qquad \textbf{35}$$

Using Equation 21 and assuming that $V_l(t=0)$ and ε_o are not a function of y,

$$V_l\,(t = 0) = \frac{Q}{2NWe_o \sum_{i=1}^{ny} \Delta y} \qquad \textbf{36}$$

After the suspension flow rate at t=0 is known, then the parameter "b" in Equation 34 can be determined from

$$b = \frac{me}{k} V_l(t = 0) \qquad \textbf{37}$$

where k and ε are evaluated at $p_{initial}$. Once the parameter “b” is known, then the initial parabolic distribution of porosity (or pressure) is known.

The following steps were performed in the numerical solution at the end of each time step:

- The liquid velocity is computed from Equation 34.
- The filtrate production is then computed from Equation 21.
- The applied porewater pressure is determined from Equation 18.
- The porosity at z=0 is calculated from Equation 25 for the exponential constitutive relationship.
- The ADI technique is used to solve for the new porosity distribution at the next time step.

MODEL RESULTS

To demonstrate the model solution, a set of model parameters and constitutive relationships were chosen. Table 1 shows the operational parameters for the simulation, and Table 2 shows the assumed slurry properties. Table 3 shows those parameter values that were derived from the operational and the slurry parameters. The initial porosity and porewater pressure distribution were shown in Figures 6 and 7 using a value of “b” of 14 kPa/cm^3/s. Figure 9 shows the predicted filtrate production over time for this simulation. Figure 10 shows the predicted porosity distribution after 60 s. Since the porosity distribution predicted by the model was largely one-dimensional in the z-axis, this simulation result may have been successful using just a one-dimensional, rather than a two-dimensional model. The tendency to a one-dimensional solution is a result of both the assumed initial porosity distribution and the isotropy of permeability in y and z.

Table 1. Operational variables for a filter plate simulation.

Operational variables	**Symbol**	**Assumed value**
Applied pressure differential at maximum pressure	$P_{applied}$	690 kPa
Pressure after filtration cell is filled	$P_{initial}$	175 kPa
Cell length	$\sum_{ny} \Delta y$, where ny is the number of grid cells in the y-direction, L	50 cm
Half cell height	$\sum_{nz} \Delta z$, where nz is the number of grid cells in the z-direction, H	50 cm
Grid points in y	ny	50
Grid points in z	nz	50
Supply pump characteristic curve parameter	p_a (Equation 18)	690 kPa
Supply pump characteristic curve parameter	p_b (Equation 18)	-1.3 kPa / cm^3 / s
Supply pump characteristic curve parameter	p_c (Equation 18)	-0.055 kPa / cm^6 / s^2
Number of plates	N (Equation 21)	100
Width of cell	W (Equation 21)	5 cm
Inlet half width	(see Figure 1)	10 cm

Table 2. Slurry properties for a filter plate simulation.

Slurry variables	**Symbol**	**Assumed value**
Effective-stress - porosity relationship parameter	ava_y=ava_z (Equation 22)	2.04E-15 g / cm / s^2
Effective-stress - porosity relationship parameter	avb_y=avb_z (Equation 22)	28.9 [-]
Permeability - porosity relationship parameter	pka_y=pka_z (Equation 23)	2.04E-16 cm^2
Permeability - porosity relationship parameter	pkb_y=pkb_z (Equation 23)	28.9 [-]
Suspension temperature	T, the temperature of the slurry affects the dynamic viscosity	27^oC
Initial porosity of slurry	ε	0.85 [-]

Table 3. Derived variables for a filter plate simulation.

Derived variables	**Symbol**	**Assumed value**
Pressure initial condition shape parameter	b (Equation 32)	14 kPa/cm
Pressure initial condition shape parameter	c (Equation 32 and 33)	-0.28 kPa/cm^2
Initial filtrate velocity at initiation of filtration	V(y,z=0,t=0) (Equation 34 and 35)	0.006 cm/s
Initial porosity at z=0 at t=0 at Pinit of 175 kPa	ε(z=0, t=0)	0.56 [-]
Terminal porosity at p=690 kPa	ε_o	0.51 [-]

In order to show the influence of the relationship of k_y to k_z on model results, Figures 11 and 12 show porosity profiles after 60 s for k_y/k_z=10 and k_y/k_z=100, respectively. For these simulations shown in Figures 11 and 12, the same parameter values were used in Tables 1 and 2 except that the value of pkya was increased by a factor of 10 and 100, respectively. The predicted impact of anisotropic permeability resulted in somewhat different predicted distributions of cake porosity. Calculations of the predicted velocity field and streamlines are shown in Figures 13 and 14 for k_y/k_z=10 and k_y/k_z=100, respectively, after 60 s. The predicted velocities were highest at the inlet and were affected significantly by the ratio of lateral to vertical permeability. The predicted rate of filtrate volume production though was the same for these simulations as for the case of k_y/k_z=1 since k_z was not changed between runs.

CONCLUSIONS

A numerical model of the filtration dynamics of a plate-and-frame press was developed. How the model parameters could be used to solve the governing equations was demonstrated. The model was especially sensitive to the assumed initial porosity distribution at the end of the filling cycle and to the chosen constitutive parameter values. Our understanding of the basic slurry constitutive properties is essential to model filtration processes adequately. Whether there are spatial anisotropies in permeability is also an area of research since it affects the predicted porosity and velocity distribution within the cake.

The model is not applicable prior to filling the filtration cell since inertial and solid-solid shear stress terms may be important and is also not applicable to very small pressure differentials where gravity forces may become important. Since the initial parabolic distribution of applied pressure (Equation 32) was chosen for mathematical convenience, the validity of this assumption also needs to be evaluated further.

REFERENCES

Anderson, D. A.; Tannehill, J. C.; and Pletcher, R. H. (1984) Computational Fluid Mechanics and Heat Transfer, Hemisphere Publishing Company, New York.

Avery, L. (1988) “Latest Developments of Diaphragm Plate Filter Presses and Other Variable Volume Filters,” Proceedings International Technical Conference on

Filtration and Separation, American Filtrations Society, Ocean City Maryland, pp. 583-602.

Vorobjov, E. (1993) Personal communication, Sugar Research Institute, Kiev, Ukraine.

Vorobjov, E. I.; Anikeev, J. V.; and Samolyotov, V. M. (1993) Dynamics of filtration and expression: new methods for combined analysis and calculation of the process with due account of the cake consolidation dynamics and the filter medium compressibility, Chemical Engineering and Processing, Vol 32, 45-51.

Wells, S. A. (1991) " Two-Dimensional, Steady-State, Modeling of Cake Filtration in a Laterally Unconfined Domain," Fluid/Particle Separation Journal, Vol. 4, No. 2, 107-116.

Willis, M. S. (1983) “A Multiphase Theory of Filtration,” Progress in Filtration and Separation, ed by R. Wakeman, Elsevier Scientific.

Acknowledgments: Appreciation is expressed to Dr. Eugene Voroboyov for many helpful discussions at the Sugar Research Institute, Kiev, Ukraine while the author was a Fulbright Scholar at the Ukrainian State University of Food Technology. Those who contributed to the success of this project at the Ukrainian State University included Dr. Ivan Malejik, chairman of the Food Processing Cathedra, Dr. Leonid Bobrivnik, Vice-Rector and Chief of Research, and Dr. Ivan Guhly, Rector of the University.

Figure captions

Figure 1. Layout of a plate-and-frame press filtration cell.

Figure 2. Characteristic curve for plate-and-frame pump where P_{max} is 690 kPa. The characteristic curve parameters from Equation 18 were p_a=690 kPa, p_b=-1.3 kPa/cm^3/s and p_c=-0.055 kPa/cm^6/s^2.

Figure 3. Variation of effective stress with porosity for constitutive relationships using the exponential form (Equation 22) and the power-law form (Equation 27). The following parameter values were used: ava=2.1E-11 kPa-1, avb=28.9[-]; Go=6900 kPa, n=1, σ_{small}=0.007 kPa.

Figure 4. Variation of permeability with porosity for constitutive relationships using the exponential form (Equation 23) and the power-law form (Equation 26). The following parameter values were used: pka=2.1E-16 cm^2, pkb=18[-]; r_o=1E14 m^2, S=0.5, σ_{small}=0.007 kPa.

Figure 5. Effect of variation of σ_{small} on the effective stress-porosity relationship using the power-law constitutive function.

Figure 6. Variation of porewater pressure with distance from the filter medium (z=0 is at the filer medium and z=1 is at the centerline of the cell) as a function of the parameter “b” [kPa/cm] in Equation 32 for an initial pressure differential of 175 kPa.

Figure 7. Variation of porosity with distance from the filter medium (z=0 is at the filter medium and z=1 is at the centerline of the cell) as a function of the parameter

“b”[kPa / cm] in Equation 32 for a pressure differential of 175 kPa and using Equation 25 with ava=2E-12 kPa, avb=28.9, and ε_i=0.85.

Figure 8. Variation of filtrate velocity at z=0 as a function of the parameter “b” using Equation 34 with Equation 23 (pka=2.1E-16 cm^2, pkb=18[-]) for a pressure differential of 175 kPa.

Figure 9. Predicted filtrate production for simulation based on parameters in Tables 1 and 2.

Figure 10. Predicted porosity distribution after 60 s for simulation based on parameters in Tables 1 and 2.

Figure 11. Predicted porosity distribution after 60 s for simulation based on parameters in Tables 1 and 2 except that k_y / k_z=10.

Figure 12. Predicted porosity distribution after 60 s for simulation based on parameters in Tables 1 and 2 except that k_y / k_z=100.

Figure 13. Predicted fluid velocity distribution after 60 s for simulation based on parameters in Tables 1 and 2 except that k_y / k_z=10. Streamlines are shown illustrating the fluid path through the cake.

Figure 14. Predicted fluid velocity distribution after 60 s for simulation based on parameters in Tables 1 and 2 except that k_y / k_z=100. Streamlines are shown illustrating the fluid path through the cake.

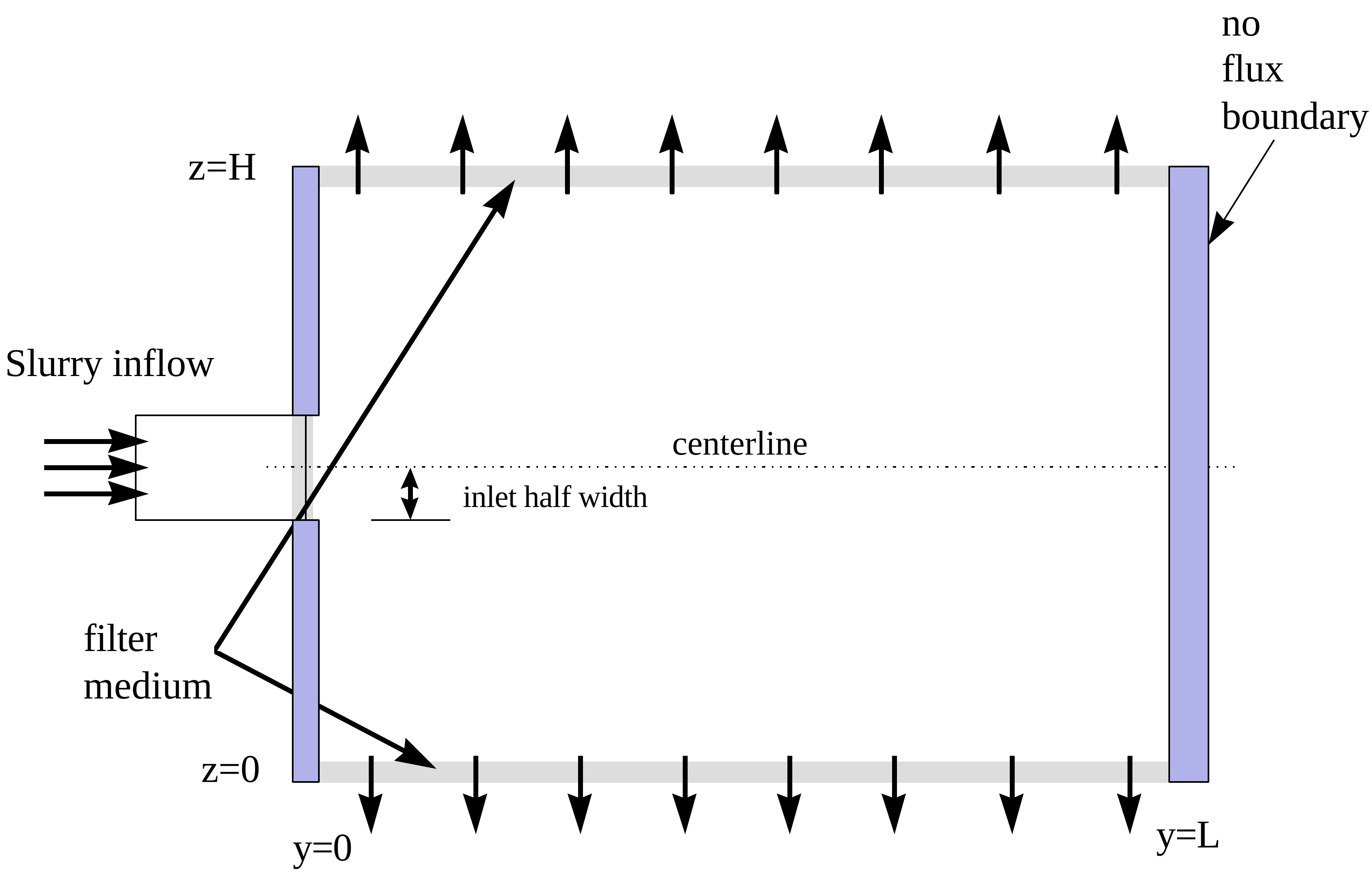
no
flux
boundary
z=H
Slurry inflow
centerline
inlet half width
filter
medium
z=0
y=0
y=L

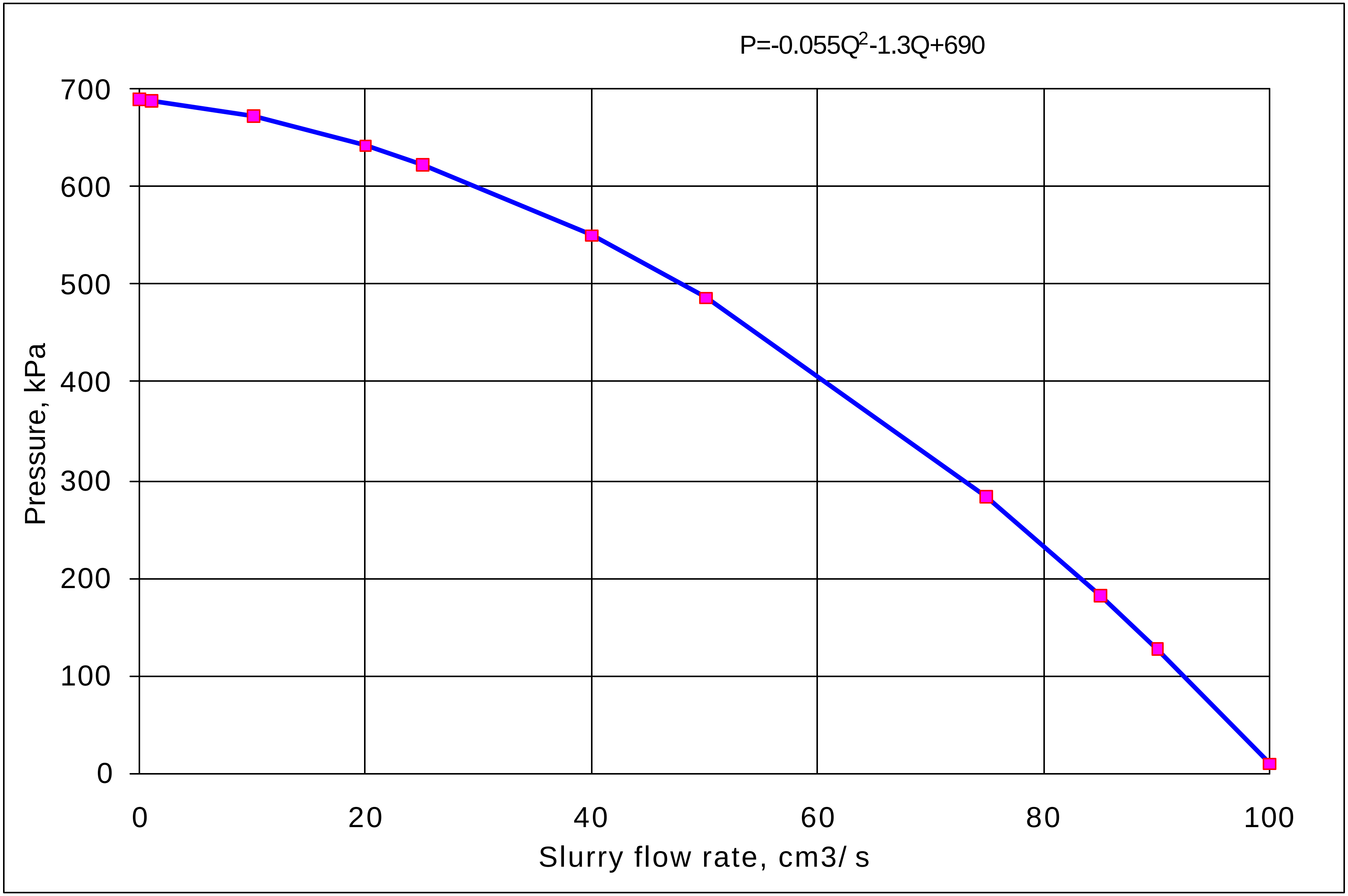
P=-0.055Q2-1.3Q+690
Pressure, kPa
700
600
500
400
300
200
100
0
0
20
40
60
80
100
Slurry flow rate, cm3/ s

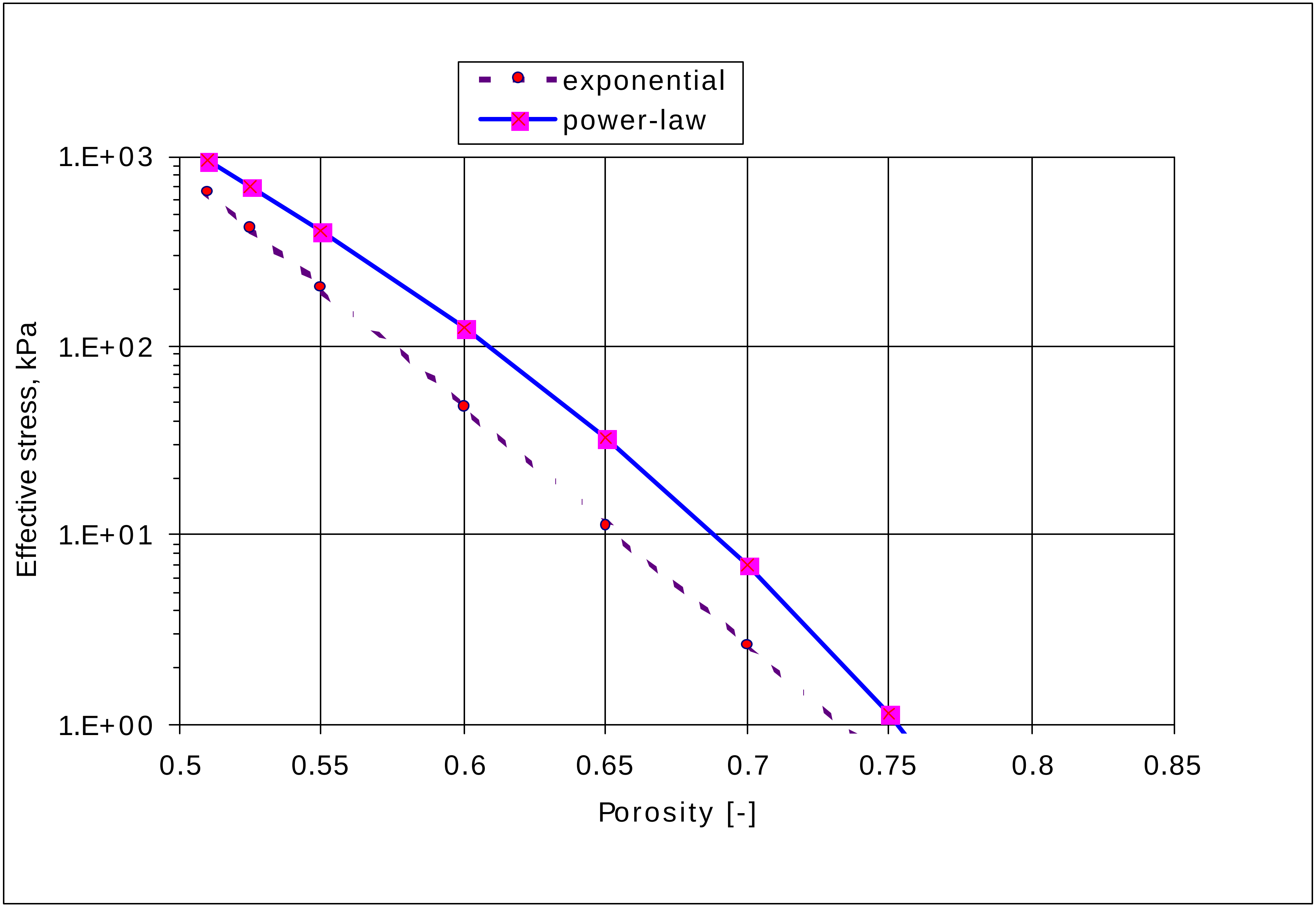

exponential
power-law
1.E+03
1.E+02
1.E+01
1.E+00
Effective stress, kPa
0.5
0.55
0.6
0.65
0.7
0.75
0.8
0.85
Porosity [-]

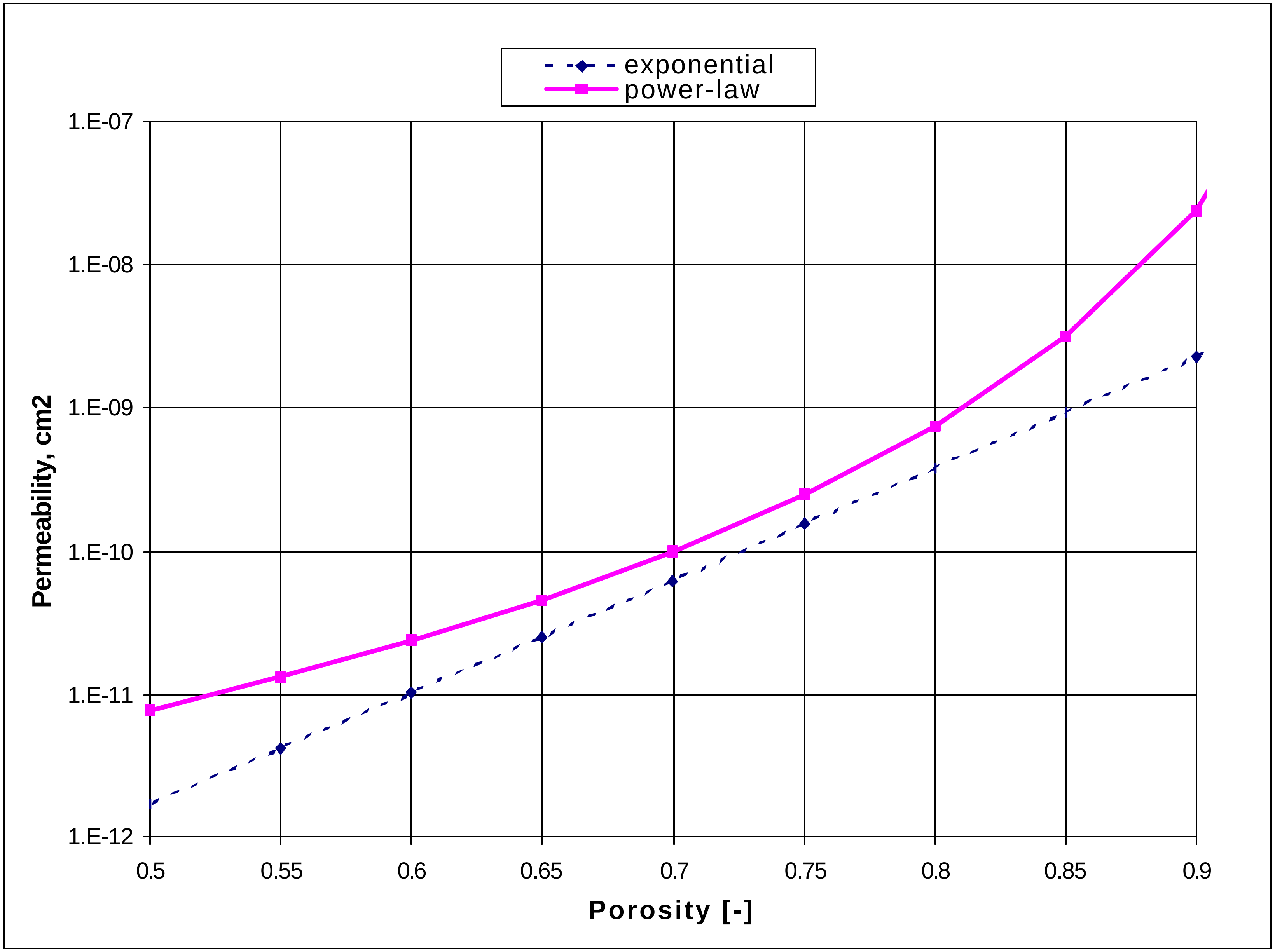
exponential
power-law
1.E-07
1.E-08
1.E-09
1.E-10
1.E-11
1.E-12
Permeability, cm2
0.5
0.55
0.6
0.65
0.7
0.75
0.8
0.85
0.9
Porosity [-]

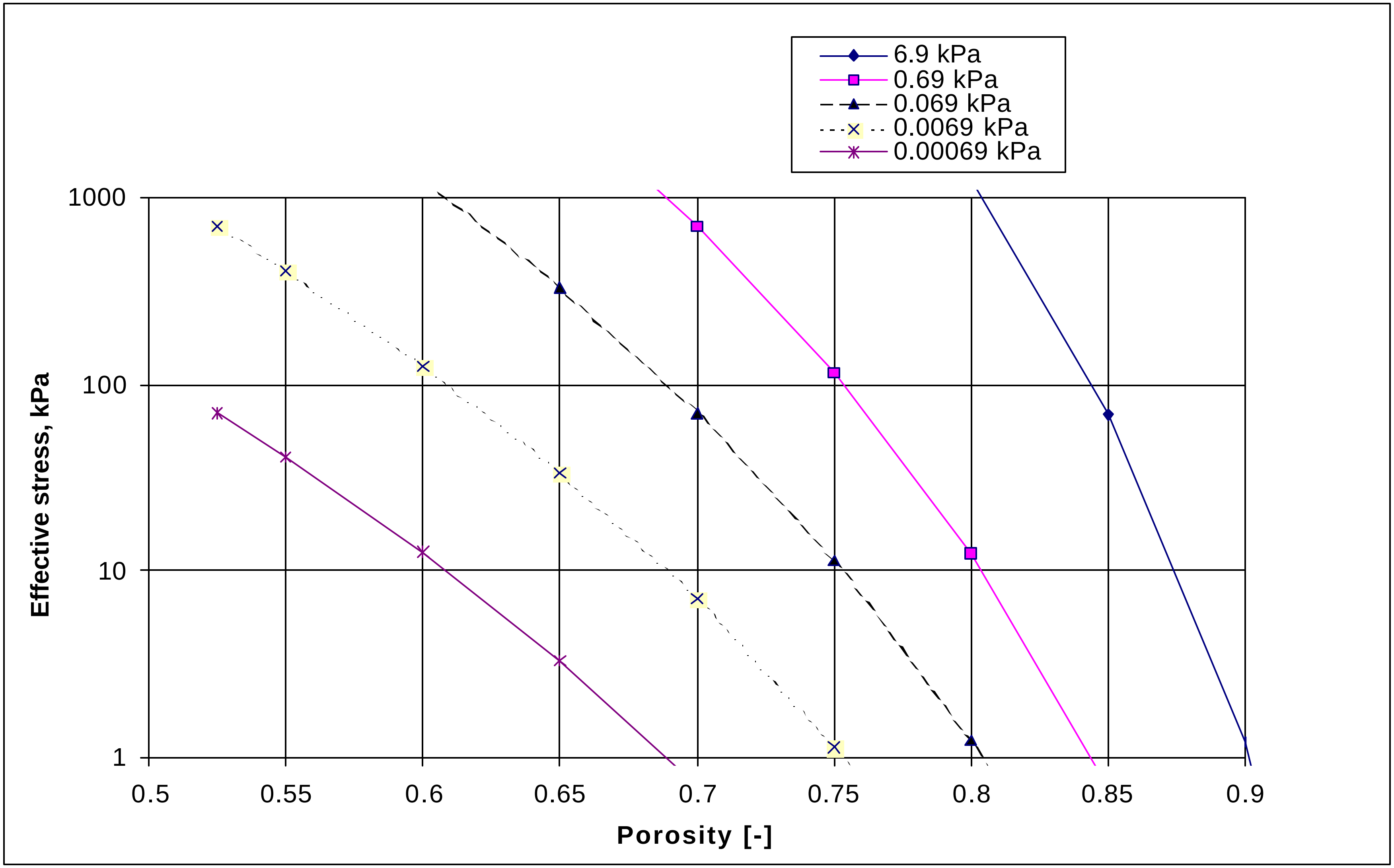
6.9 kPa
0.69 kPa
0.069 kPa
0.0069 kPa
0.00069 kPa
1000
100
10
1
0.5
0.55
0.6
0.65
0.7
0.75
0.8
0.85
0.9
Porosity [-]
Effective stress, kPa

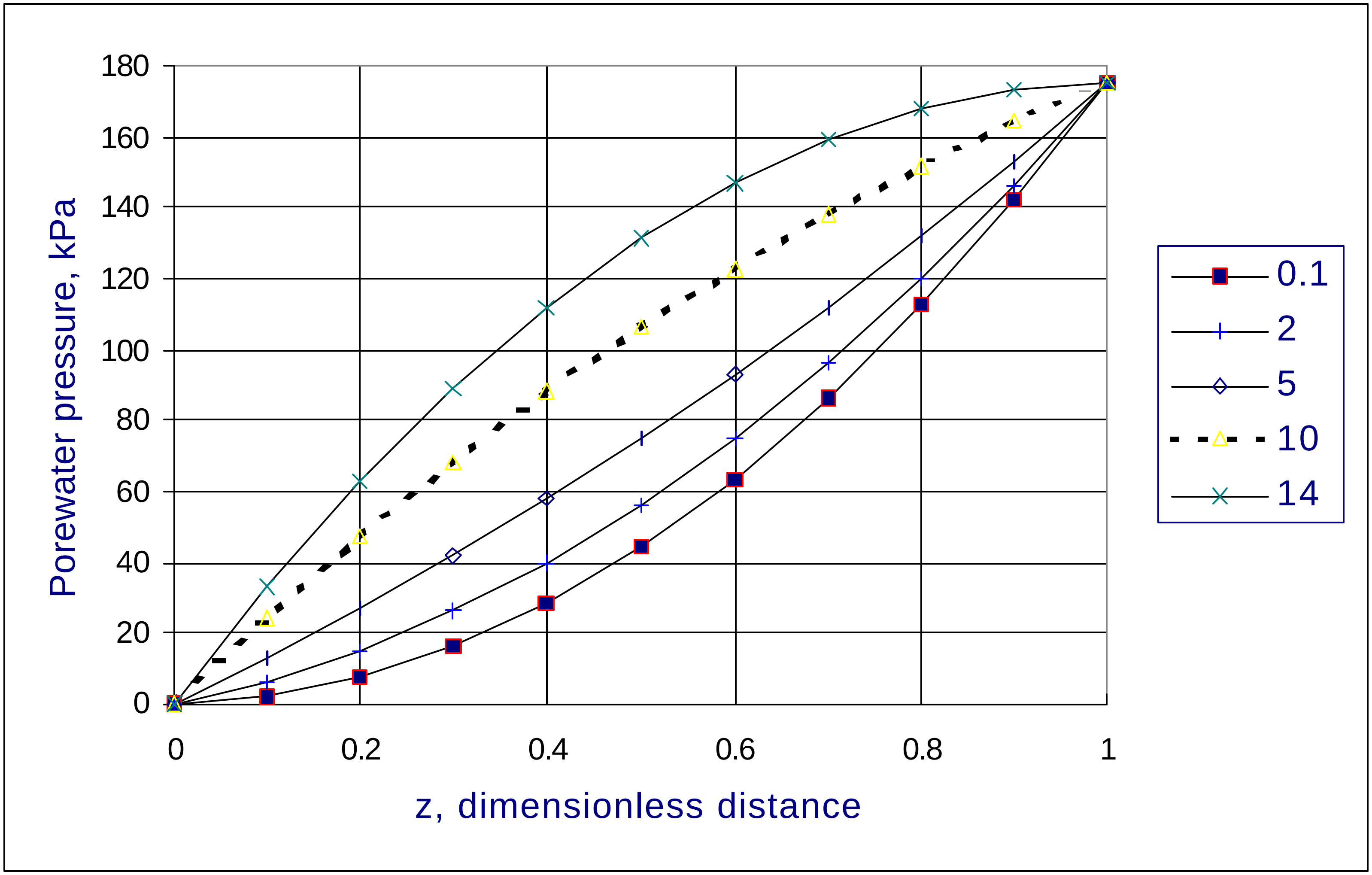

Porewater pressure, kPa
180
160
140
120
100
80
60
40
20
0
0
0.2
0.4
0.6
0.8
1
z, dimensionless distance
0.1
2
5
10
14

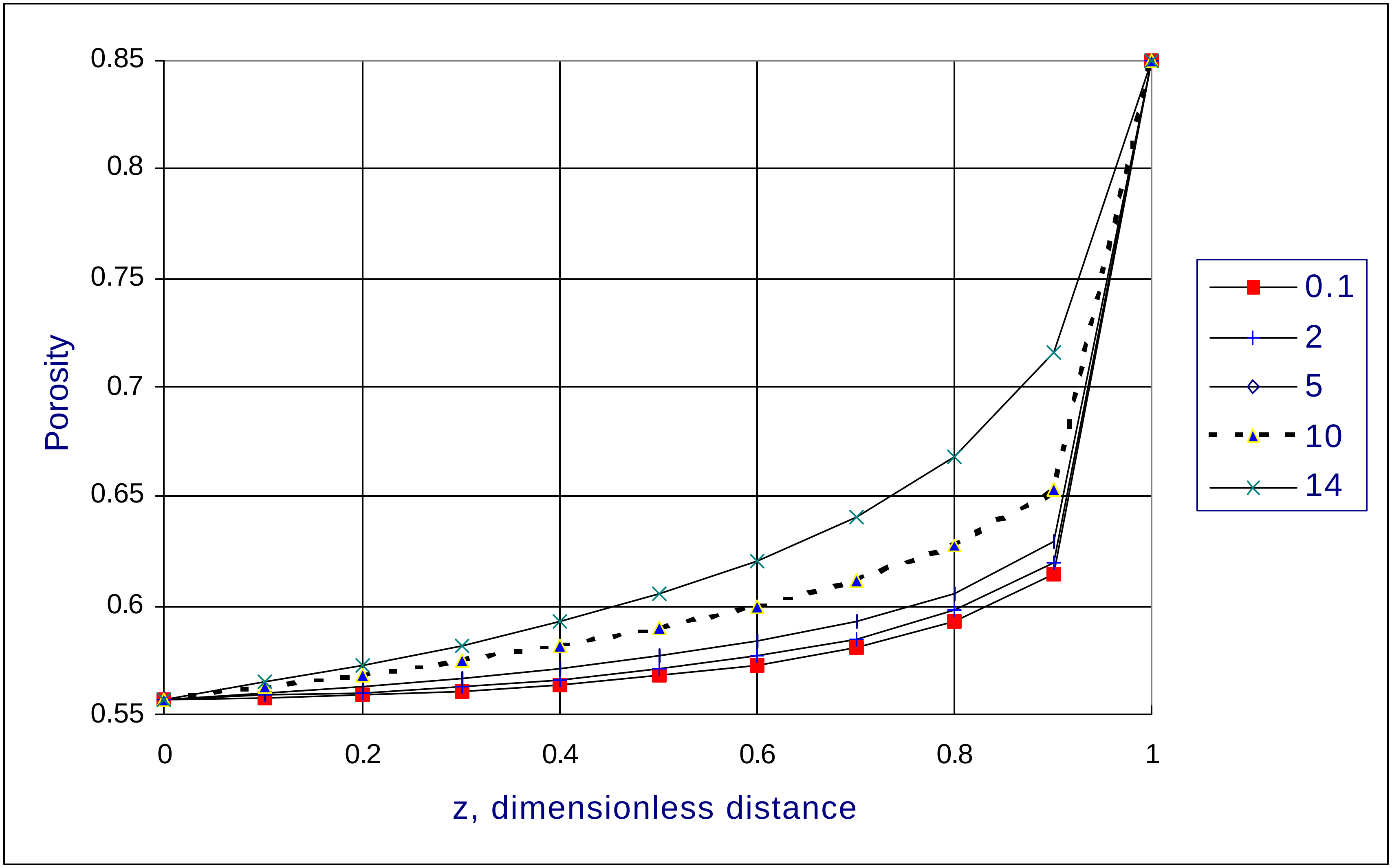

0.85
0.8
0.75
0.7
0.65
0.6
0.55
Porosity
0
0.2
0.4
0.6
0.8
1
z, dimensionless distance
0.1
2
5
10
14

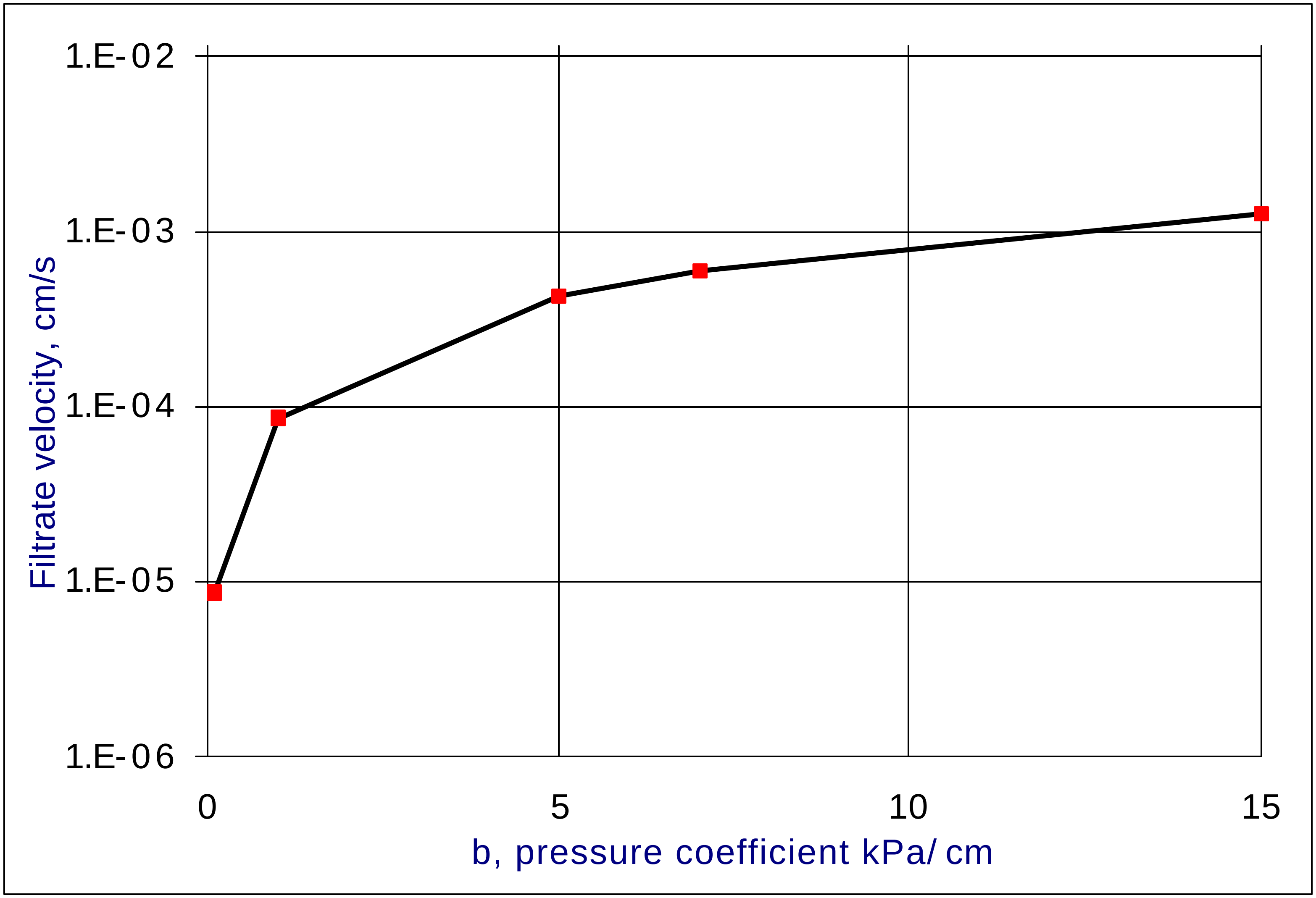
1.E-02
1.E-03
1.E-04
1.E-05
1.E-06
Filtrate velocity, cm/s
0
5
10
15
b, pressure coefficient kPa/ cm

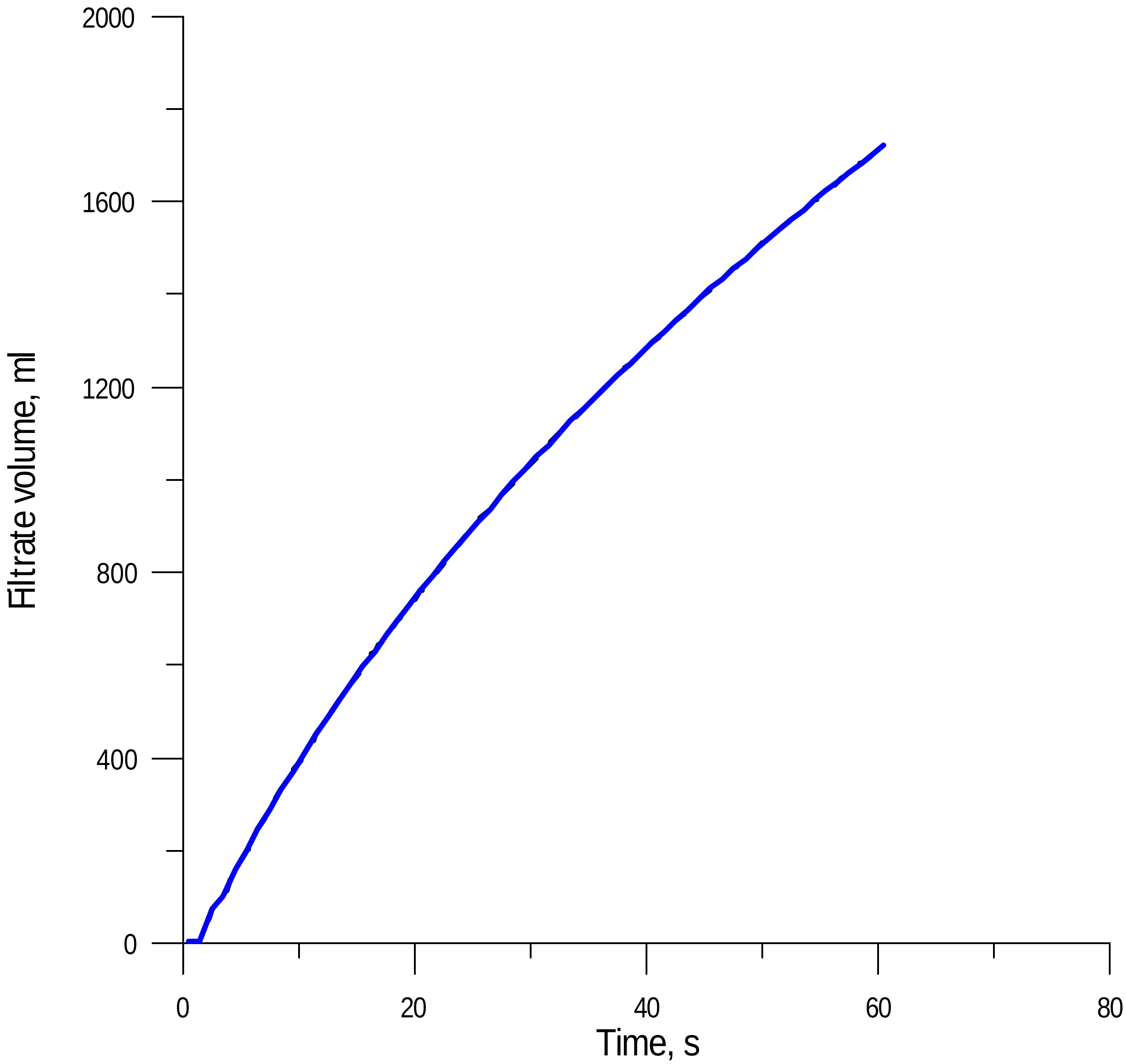

2000
1600
1200
800
400
0
Filtrate volume, ml
0
20
40
60
80
Time, s

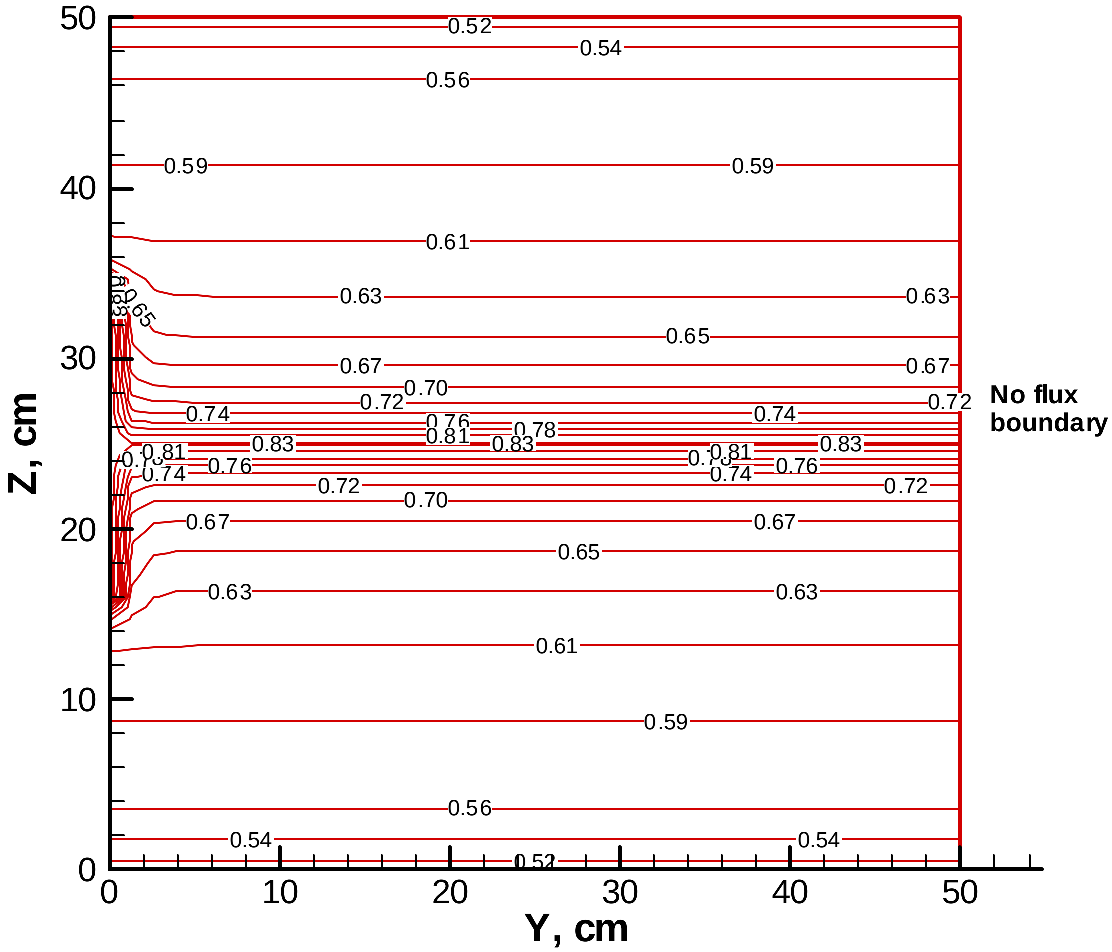

0.52
0.54
0.56
0.59
0.61
0.63
0.65
0.67
0.70
0.72
0.74
0.76
0.78
0.81
0.83
No flux boundary
Z, cm
Y, cm
0
10
20
30
40
50

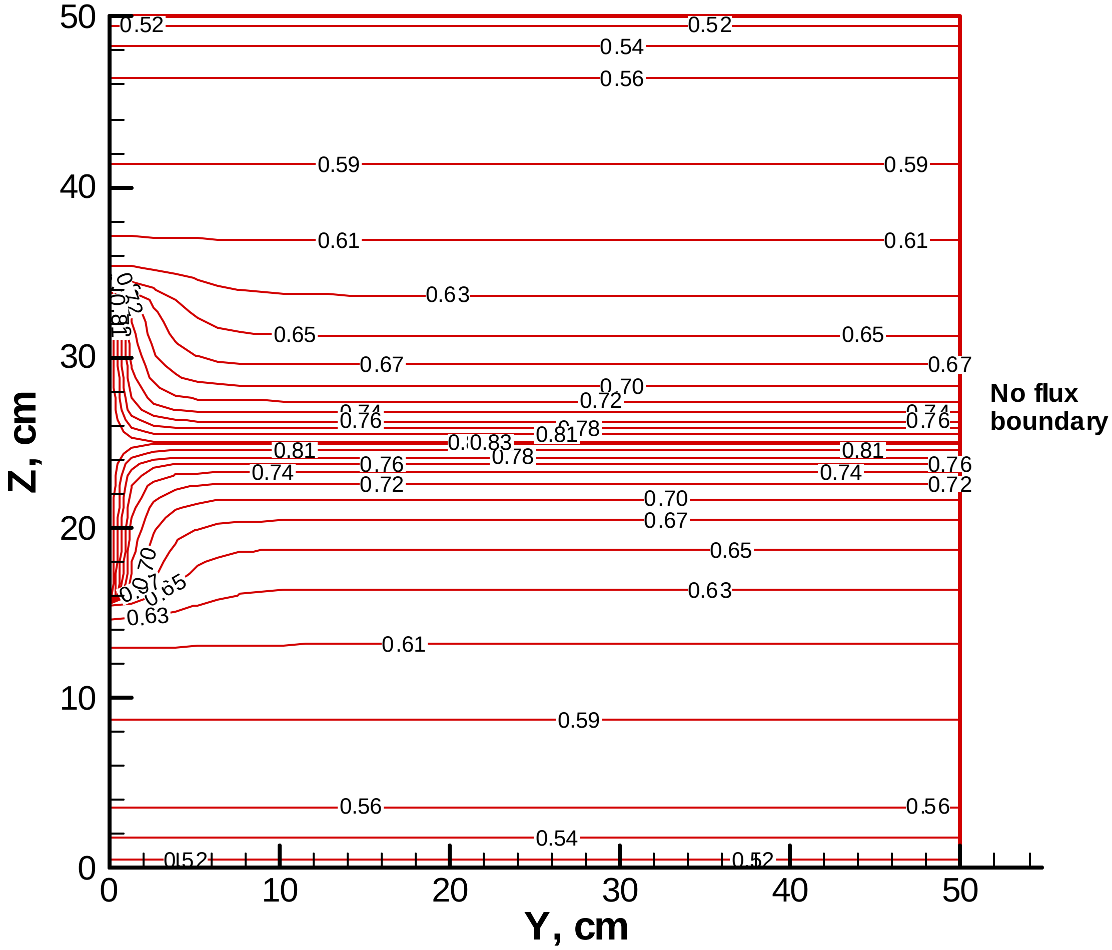

No flux boundary
Z, cm
Y, cm
0
10
20
30
40
50
0.52
0.54
0.56
0.59
0.61
0.63
0.65
0.67
0.70
0.72
0.74
0.76
0.78
0.81
0.83

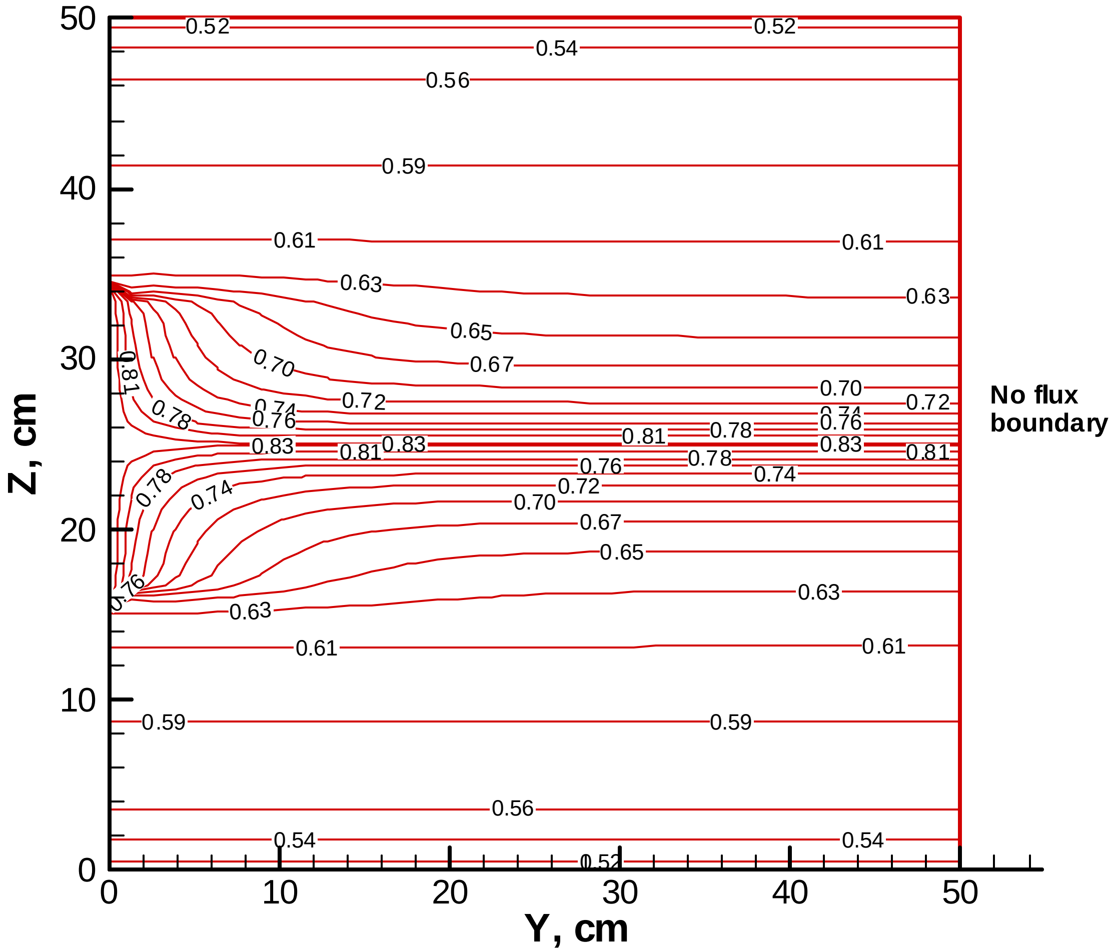
No flux
boundary
Z, cm
Y, cm
0.52
0.54
0.56
0.59
0.61
0.63
0.65
0.67
0.70
0.72
0.74
0.76
0.78
0.81
0.83

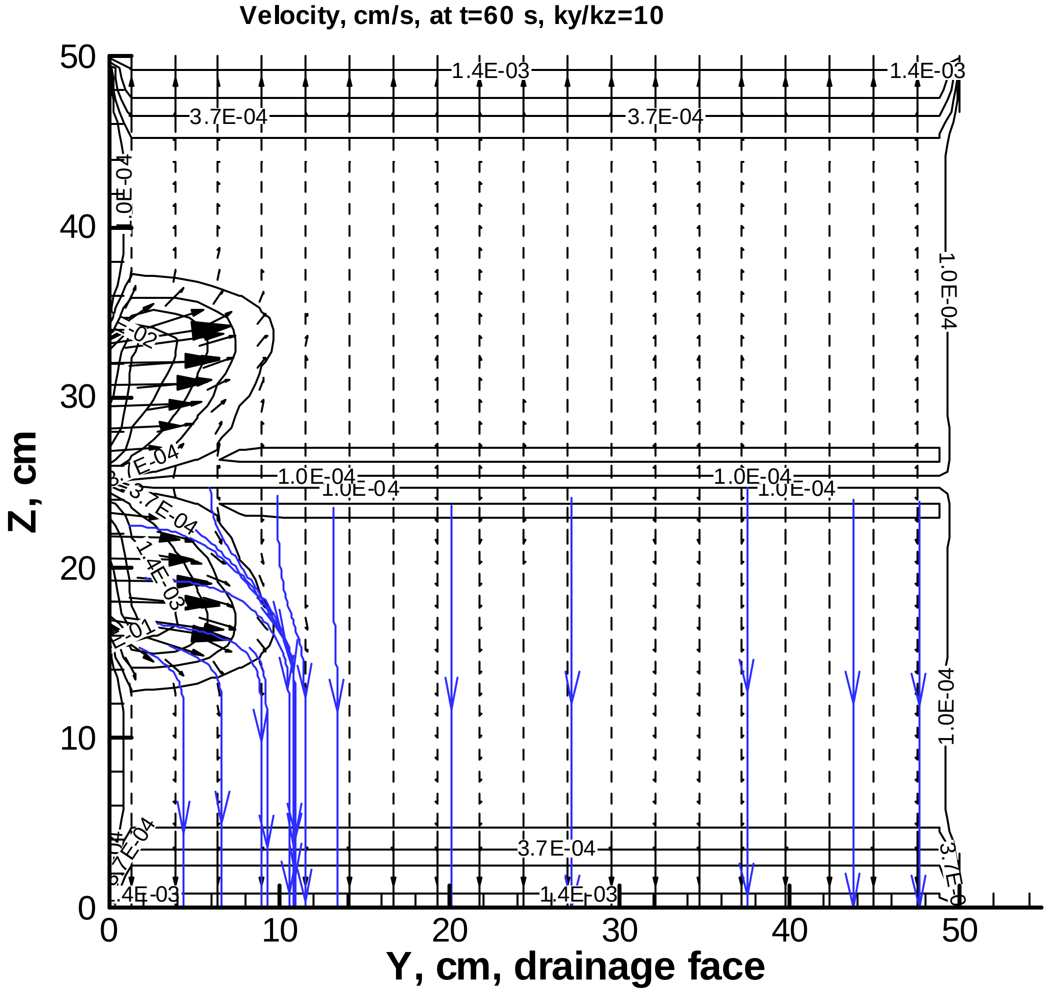
Velocity, cm/s, at t=60 s, ky/kz=10
Z, cm
Y, cm, drainage face
1.4E-03
3.7E-04
1.0E-04
0
10
20
30
40
50

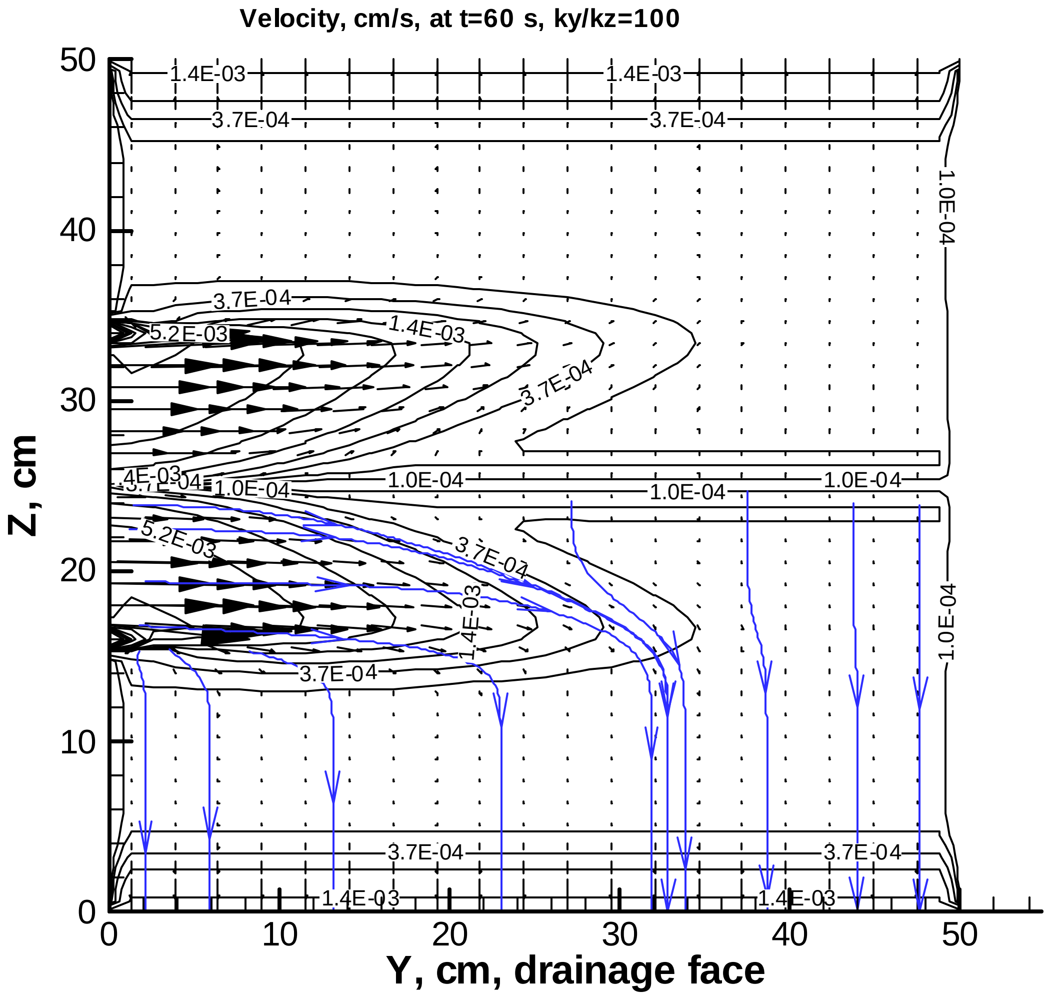
Velocity, cm/s, at t=60 s, ky/kz=100
Z, cm
Y, cm, drainage face
0
10
20
30
40
50
1.4E-03
3.7E-04
1.0E-04
5.2E-03